Computational Study on Dynamic Stall and Flow Control in a Pitching Airfoil

Patibandla B. L. V. Ramana, Akshoy Ranjan Paul, Anuj Jain, and Kazuo Matsuura

Abstract Dynamic stall phenomenon on a Boeing Vetrol-VR-7 airfoil, oscillating at quarter chord with reduced frequency of 0.1, is investigated at three different slot configurations—leading edge, trailing edge and combination of this two edges at a Reynolds number of 2.5×10^6. It is shown that the use of a leading-edge slot can eliminate the dynamic stall vortex (DSV) and increase the lift coefficient by 20%, and a decrease in the drag and moment coefficient by more than 70%. It is computed that the performance at low angles of attack can be improved with the use of a non-drooped leading edge in the airfoil. Furthermore, the combination of a leading and trailing-edge slots further improves the lift characteristics.

Keywords Pitching airfoil · Leading-edge slot · Reduced frequency · Dynamic stall · Leading-edge vortex (LEV) · Dynamic stall vortex (DSV)

1 Introduction

A phenomenon that is frequently encountered in airfoils whose angle of attack (AoA) oscillates with respect to free stream velocity, like in advancing rotorcrafts, jet compressors, wind turbines, rapid maneuvering aircraft, birds and insects, is called dynamic stall. It can be characterized by an increase of lift beyond static stall angle and a sudden loss of moment coefficient followed by lift coefficient after a particular dynamic stall angle. In static stall, however, lift and moment stall occur simultaneously. This sudden drop in moment and lift coefficients causes fluctuating loads on airfoils, which leads to fatigue and flutter, which could be detrimental to structural integrity and life of rotor blades, wind turbines, etc. [1, 2].

P. B. L. V. Ramana · A. R. Paul (✉) · A. Jain
Department of Applied Mechanics, Motilal Nehru National Institute of Technology Allahabad, Prayagraj, India
e-mail: arpaul@mnnit.ac.in

K. Matsuura
Graduate School of Science and Engineering, Ehime University, Matsuyama, Ehime, Japan

Dynamic stall occurs by formation and shedding of a dynamic stall vortex (DSV) which results in a sudden increase and an immediate drastic decrease in lift. This DSV forms when the vorticity flux level exceeds a limit threshold. It can be understood by the following equation:

$$\nu \frac{\partial \omega}{\partial n} = \frac{\partial U_s}{\partial t} + \frac{1}{\rho} \frac{\partial P}{\partial n} + \nu \omega \qquad (1)$$

Here, the LHS is the vorticity flux, where ν is kinematic viscosity, n is the direction normal to the surface of the airfoil, and ω is spanwise vorticity. The first term in the RHS is the surface acceleration term, where U_s is the surface tangential speed, while the second term is the pressure gradient term, where s is the direction along the surface, ρ is density of the fluid and the third term is surface transpiration term. During pitching motion, the vorticity flux increases rapidly, this vorticity coalesces after a threshold and forms a dynamic stall vortex (DSV). Therefore, DSV manipulation involves not letting the vorticity to coalesce by shedding smaller pieces of this vorticity into the wake. Then the consequences of vortex induced fluctuating loads can be reduced. This can be done either by surface acceleration or by injecting or extracting fluid from the flow field as per the equation above [3].

One of the most efficient passive methods of injecting and extracting fluid from the flow field is with the help of slots on the airfoil. Slotted airfoils are independently developed by Lachman [4] to reduce flow separation and increase stall angle. These slots divide the airfoil into parts. In a three-part wing, there are two slots—one at leading edge and the other at trailing edge. The leading-edge part is called a 'slat,' the middle part is called 'main element' or 'main airfoil' and the trailing-edge part is called a 'flap.'

The major mechanisms responsible for the effectiveness and lift increasing capability of these instruments are (a) Slat effect: Reduction in the circulation of the main element because of the circulation of the slat. (b) Circulation effect: The circulation of the slat is increased by the effect of the main airfoil. (c) Dumping effect: Slat boundary is dumped at high velocity, which will reduce separation and increase lift. (d) Off the surface pressure recovery: Deceleration of the flow and pressure recovery occurs in the free stream. (e) Fresh boundary layer effect: As every element experience a new thin boundary layer, it can withstand higher adverse pressure gradient. A detailed description of all these effects is given by Smith [5].

The first use of a leading-edge slat in a dynamic stall situation is in 1983 research paper of Carr and McAlister [6]. They have used a VR-7 airfoil with a NACA 15320 slat pitching around the quarter chord. Different parameters like Reynolds number (Re), mean AoA, reduced frequency (k) were varied. The dynamic stall reappeared after mean AoA of 20° even in slatted airfoil. In basic airfoil at Mach number = 0.185, Re = 2.5×10^6, $k = 0.1$ and for AoA varied as $15° + 10° \sin(\omega t)$, reversed flow reached leading edge at AoA of 22°. However, in slatted case, it barely reached quarter chord at all. Later, McAlister and Tung [7], Tung et al. [8] and Tuncer and Sankar [9] carried out further investigation using Boeing Vetrol-VR-7 airfoil.

Van Dam [10] produced a comprehensive review of multi-element airfoils used for transport airplane application. It was observed that even though these aircrafts operate at high Reynolds numbers, because of the relatively small size of slats, the Reynolds number on the slat is still laminar. Therefore, transition modeling is an important aspect for multi-element airfoil modeling.

It is observed from literature review that very few slat geometries are tested for dynamic stall. Most of these slats, being drooped, produced high drag and less lift during low angle of attacks because of the increase in zero-lift angle of attack. Moreover, only a few researchers have implemented a non-drooped slat and conducted optimization study regarding the slats. Hence, a non-drooped slat (using a leading-edge slot) is tested in the present study along with a trailing-edge slot and a combination of both to test the efficiency of slots at two different locations. The following section describes the computational techniques, which includes geometry, grid generation and the solver settings.

2 Computational Methodology

If equations are present, they should be numbered in the order of appearing, and all symbols and variables described.

2.1 Geometry

The airfoil used in this work is a Boeing Vetrol-VR-7 airfoil with a trailing-edge 'tab.' Tabs are instruments connected at the end of an airfoil used to decrease camber and reduce pitching moment. The chord length of the airfoil is 0.61 m and the airfoil is placed at an initial AoA of 15°. The outlet angle, cutoff length and chord length of leading-edge and trailing-edge slot positions are 20°, 6.4% chord, 12% chord and 36°, 70% chord, 8% chord, respectively, and are as depicted in Fig. 1a. 6.4% cord is the position of the stagnation point at 20° AoA (2° before stall). Most of the other parameters are chosen from Greenman and Roth [11]. Only slot gap of 1% chord is used to position the slat and flap away from the main element along the chord line.

An O-type computational domain is divided into inner and outer regions. The inner region is a circular zone around the airfoil at a radius of 5 chord length. A sliding mesh technique is used to give pitching motion for the inner zone. The outer region is a stationary zone of radius 20 chord length.
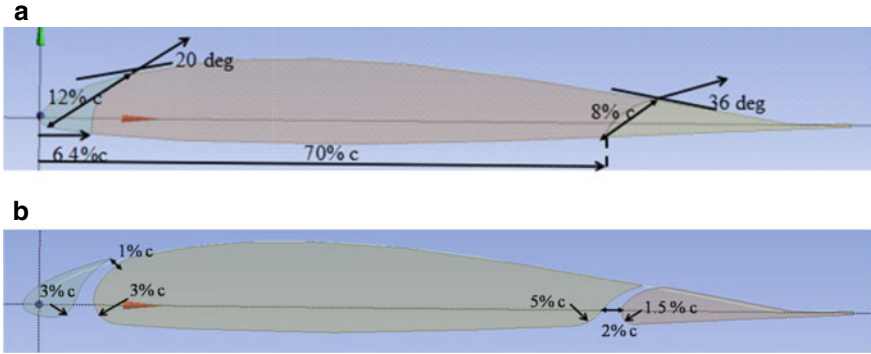
Fig. 1 **a** Slot location and geometry. **b** Slot position and geometry

2.2 Grid Generation

A hybrid mesh is generated, using Ansys-ICEM 16.0, for all the cases tested with quadrilateral, near wall cells and triangular cells away from the wall. First cell height of 5×10^{-6} is used with a y^+ value less than 1. In the near wall boundary layer region, 70 nodes perpendicular to the airfoil are used to resolve the flow reversal and reattachment. This inflation layer is as shown in Fig. 2a. The equi-angle skewness of all the meshes is above 0.3 indicating good quality. The equi-angle skewness of all the meshes is above 0.3 indicating good quality.

Grid independence test is carried out on a non-slotted airfoil, as it is computationally prohibitive to carry the same test on all the other conditions. As there is sufficient literature [12, 13] on the grid independence tests, the element sizes on different zones, considered optimum by those works, are chosen. Three different time-step size (t/T = 0.01, 0.005, 0.0025) are chosen for the time-step independence study.
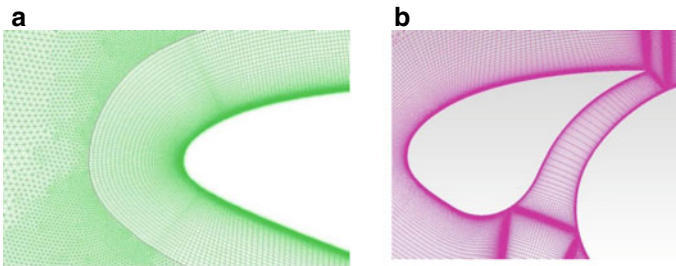

Fig. 2 **a** Inflation layer. **b** Meshing in the slot

2.3 Governing Equations and Boundary Conditions

The governing differential equations of this unsteady flow phenomenon are unsteady Navier–Stokes equations along with continuity and energy equations. Shear stress transport (SST) k-ω turbulence model is used in the present study because this turbulence model was widely used for dynamic stall prediction, for modeling adverse pressure gradients [10, 12, 13] and for grid and time convergence studies [13, 14].

An airfoil, oscillating from $5°$ to $25°$ with a reduced frequency of 0.1, freestream Mach number of 0.185 and $Re = 2.5 \times 10^6$ is used to study the slot flow control of dynamic stall. Pressure far field along with inlet Mach number is used as the inlet boundary condition. Pressure outlet option is used as outlet boundary condition and the border between inner and outer zones is specified as an interface. No-slip boundary condition is also applied at the airfoil surface. The airfoil AoA varies in the following way:

$$\alpha = 15° - 10° \sin(\omega t)$$

Here, t is time and ω is angular frequency calculated from reduced frequency. A uniform initial flow corresponding to $Re = 2.5 \times 10^6$ everywhere in the domain is chosen.

The maximum Mach number is more than 0.3 for most of the flow around airfoil. it is observed from preliminary computational results that the area of Mach number more than 0.3 is confined to the leading edge and is very small. It is also seen that no dynamic stall vortex is visible at maximum AoA. Hence, a compressible flow solver is used from henceforth to account for and examine the effect of Mach number.

2.4 CFD Solver Settings

Coupled algorithm option available in finite-volume method-based Ansys-Fluent CFD solver is used for pressure–velocity coupling as it ensures faster convergence. Green-Gauss Node-Based methods are used for gradient evaluation as this method is more accurate for unstructured meshes. Second-order upwind spatial discretization scheme is used for all the parameters like momentum, turbulent kinetic energy, rate of turbulent dissipation and energy. The convergence criterion, for all the variables, is taken as $<\sim 10^{-5}$.
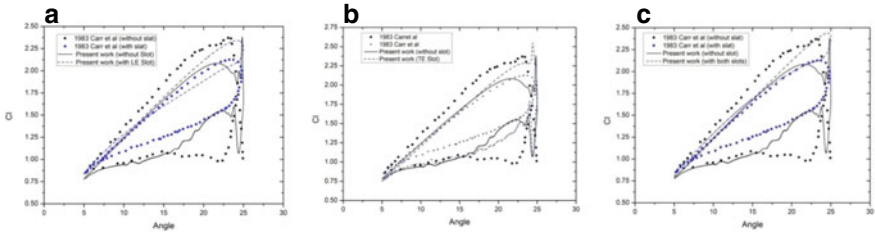
Fig. 3 **a** With LE slot. **b** With TE slot. **c** With both slots

a) 15° ↑ (Start of the cycle)

c) 24.5° ↑ (Flow separation starts)

b) 22.52 ° ↑ (Reverse flow starts)
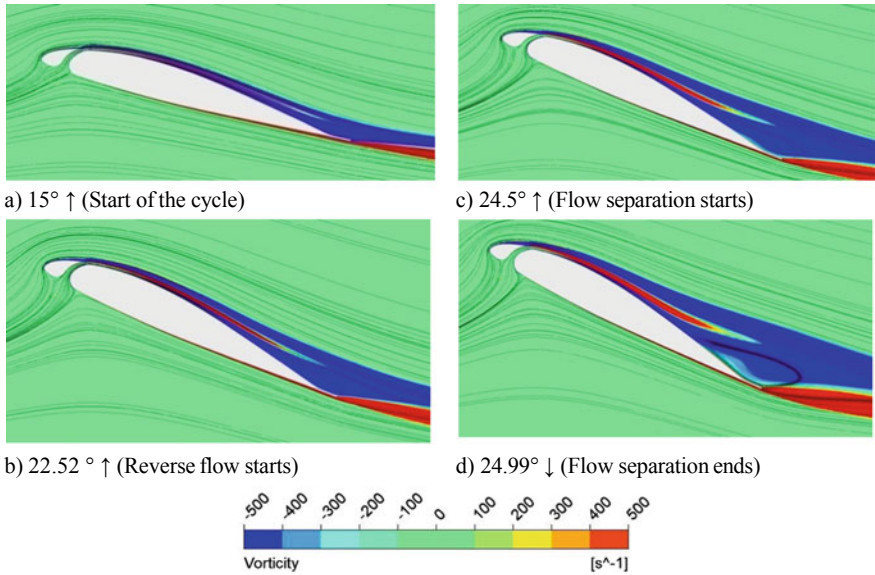
d) 24.99° ↓ (Flow separation ends)

Fig. 4 Instantaneous streamline and vorticity contour on a LE slotted airfoil

3   Results and Discussion

The work of Carr and McAlister [6] on the implementation of leading-edge slat is used for validating the computational results in the present study. The CFD results of Liggett and Smith [15] are also compared with the present results to test the efficacy of the computational method adopted here.

3.1 Leading-Edge Slot

The results of the leading-edge slot are as given in Figs. 3a and 4. In Fig. 3a, variation of lift coefficient (C_L) with AoA of VR-7 airfoil with leading-edge slot is compared with those of VR-7 airfoil with NACA 15320 leading-edge slat used by Carr and McAlister [6]. It is seen that the hysteresis loop of VR-7 airfoil with leading-edge slot is much less than the hysteresis loop of the same with a NACA 15320 slat. A small increase in lift coefficient is observed even at low AoA during the upstroke. At high AoA, because of the absence of the DSV, significant lift coefficient increase is obtained. An overall increase of 20% is observed in cycle-averaged lift coefficient with the slotted airfoil. Further, a significant decrease of 72.9 and 87% in drag coefficient and negative moment coefficient are also observed with the slotted airfoil.

However, there is separated flow on the slotted airfoil too, at higher AoA. It is observed from the vorticity contours of Fig. 4b that the boundary layer of the first element mixes with the boundary layer of the main airfoil near the trailing edge and this could be the reason for elimination of the dynamic stall. It is noticed from the instantaneous streamline diagrams (Fig. 4) that the stagnation point on the main airfoil indicates a lesser circulation around it and whereas on the first element indicates a higher circulation around it. These results agree with the mechanisms of lift increase due to slotted configuration given by Smith [5].

3.2 Trailing-Edge Slot

A trailing-edge slot is also provided in the present airfoil to check its effect on the alleviation of dynamic stall. It is observed from Fig. 3b that even though the stall is postponed to higher angles of attack with the trailing-edge slot, the stall is not eliminated. It is also seen that the lift coefficient peaks of the airfoil with trailing-edge slot are greater than the lift coefficient peaks of the basic airfoil. A 2.1% increase in the cycle-averaged lift coefficient is obtained where as an increase of 2.8 and 0.41% in drag and moment coefficients is observed. This marginal change in the aerodynamic coefficients indicates that the trailing-edge slot itself has very less impact on the dynamic stall. However, because of the slot, flows around the trailing-edge element are always attached and separate from the end of the main element.

A 4° increase in the start of the reverse flow and the reattachment time from the non-slotted airfoil is noticed From Fig. 5. However, the reverse flow reached the leading edge around the same time. The DSV and secondary vortices have shed at a larger AoA as seen in Fig. 5b. The major difference between non-slotted and trailing-edge slotted airfoil is the travel of the trailing-edge vortex. In the non-slotted case, the trailing-edge vortex travels toward the leading edge before the formation DSV, whereas in trailing-edge slotted airfoil, the trailing-edge vortex forms at the end of the main element, so it travels toward the trailing edge of the second element and then to the leading edge of the first element. This decreased the effect of separation caused
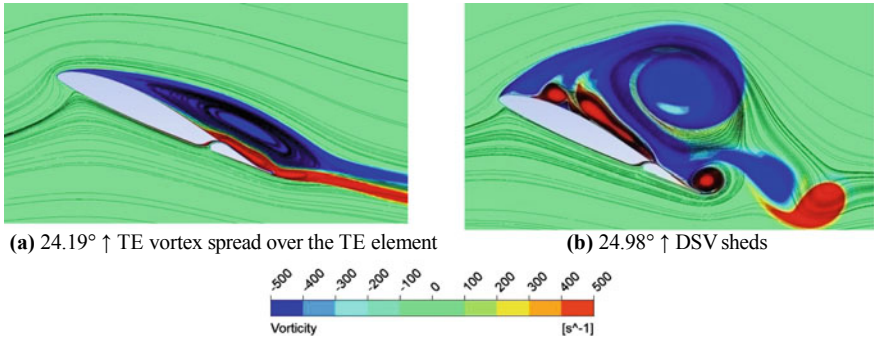
(a) 24.19° ↑ TE vortex spread over the TE element   **(b)** 24.98° ↑ DSV sheds

Fig. 5 Vorticity contour and instantaneous streamline plots of the TE slotted airfoil
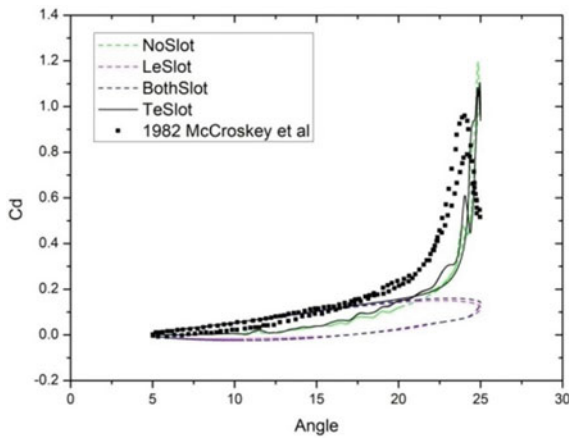

Fig. 6 Drag coefficient versus AoA of different slot configurations

by the trailing-edge vortex significantly and the first reduction in lift around 20°
observed in non-slotted case does not appear in the trailing-edge slot case (Fig. 5a).

3.3   Combination of Leading and Trailing-Edge Slots

The leading-edge slot eliminated dynamic stall vortex but a small region of flow
separation exists at high AoA. The trailing-edge slot improved the lift performance as
a result of the movement of trailing-edge vortex but could not eliminate the dynamic
stall. Based on these results, the effectiveness of the combination of both leading-edge
and trailing-edge slots is investigated. It can be observed from Fig. 3c that providing
both the slots further enhanced the lift profile. The impending trailing-edge flow
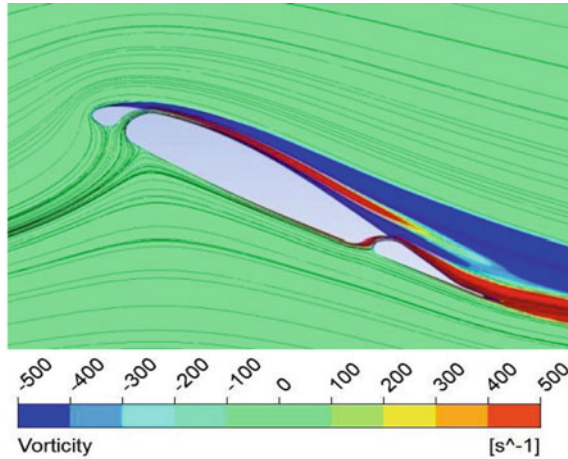separation clearly visible in the vorticity contours of the airfoil with leading-edge

Fig. 7 At 25° ↑ maximum AoA (no separation)

slot is completely absent with the addition of trailing-edge slot (Fig. 7). No stall can be observed in the figure and the cycle-averaged lift coefficient increased by 22% compared to the basic VR-7 airfoil without slots. Additionally, the cycle-averaged drag and moment coefficients reduced by 71.7% and 80%, respectively (Fig. 6).

Although the cycle-averaged lift coefficient is highest in the airfoil with both slots, it is still marginal when compared to the cycle-averaged lift coefficient of the airfoil with single leading-edge slot. Similarly, the drag coefficient versus AoA graph in Fig. 7 shows that the drag coefficient change between the airfoil with leading-edge slot and the airfoil with both slots is also marginal. It is also noticed that the influence of trailing-edge slot is minimal in reducing drag coefficient. Hence, for understanding the influence of these different slot configurations on the lift, drag and moment coefficients, the slotted airfoils need to be further tested at wider parameters and spaces.

4   Conclusions

The present work attempts at controlling the stall behavior of the VR-7 airfoil with leading and trailing-edge slots. Three slot configurations (leading edge, trailing edge and combined) on the VR-7 airfoil have been tested at 2.5 million Reynolds number and a reduced frequency of 0.1 and compared with a non-slotted VR-7 airfoil. It has been observed that the implementation of a leading-edge slot completely eliminates the dynamic stall vortex and the airfoil with leading-edge slot has a 20% higher cycle-average lift coefficient than non-slotted airfoil. The decrease in the cycle-averaged drag and moment coefficient due to leading-edge slot is more than 70% of the non-slotted values.

In the trailing-edge slotted airfoil, the stall did occur but at a higher AoA. The lift coefficient increases by 2.1% from the non-slotted case, but the drag and moment coefficients also increase by 2.8% and 0.4%, respectively. This behavior can be attributed to the distinctive feature of the trailing-edge slotted airfoil: the reverse travel of the trailing-edge vortex. The combination of both slots further increases the lift coefficient (22%), more than leading-edge slotted case, but slightly higher values of drag and negative moment are observed. The flow separation visible at a higher AoA in the airfoil with leading-edge slot is successfully eliminated by the combination of both the slots.

References

1. McCroskey WJ (1982) Unsteady airfoils. Annu Rev Fluid Mech 14:285–311
2. Carr LW (1988) Progress in analysis and prediction of dynamic stall. AIAA J Aircr 25:6–17
3. Chandrasekhara MS, Wilder MC, Carr LW (1999) Compressible dynamic stall control: a comparison of different approaches. In: 17th Applied aerodynamics conference, AIAA-99-3122
4. Lachman G (1921) Slotted wing sections. Technical notes, NACA TM-71
5. Smith AMO (1975) High lift aerodynamics. 37th Wright Brothers lecture. AIAA J Aircr 12
6. Carr LW, McAlister KW (1983) The effect of leading edge slat on dynamic stall of an oscillating airfoil. In: AIAA conference, AIAA-83-2533. https://doi.org/10.2514/6.1983-2533
7. McAlister KW, Tung C (1993) Suppression of dynamic stall with a leading edge slat on a VR-7 airfoil. NASA Technical papers, NASA-TM-3357
8. Tung C, McAlister KW, Wang CM (1993) Unsteady aerodynamic behavior of an airfoil with and without a slat. Comput Fluids 22:529–547. https://doi.org/10.1016/0045-7930(93)90024-4
9. Tuncer IH, Sankar LN (1994) Unsteady aerodynamic characteristics of a dual element airfoil. AIAA J Aircr 31:531–537. https://doi.org/10.2514/3.46526
10. Van Dam CP (2002) The aerodynamic design of multi-element high-lift systems for transport airplanes. Prog Aerosp Sci 38:101–144
11. Greenman RM, Roth KR (1999) Minimizing computational data requirements for multi-element airfoils using neural networks. AIAA J Aircr 36
12. Szydlowski J, Costes M (2004) Simulation of flow around a static and oscillating in pitch NACA 0015 airfoil using URANS and DES. In: Proceedings of HT-FED04, ASME heat transfer/fluids engineering summer conference, Charlotte, North Carolina, USA, July 2004
13. Costes M, Gleize V, Szydlowski J, Sankar LN, Guzel G, Rhee M (2005) Grid sensitivity study for the turbulent viscous flow around a NACA 0015 airfoil at stall. https://www.researchgate.net/publication/260391102
14. Richter K, Le Pape A, Knopp T, Costes M, Gleize V, Gardner AD (2009) Improved two dimensional dynamic stall prediction with structured and hybrid numerical methods. Presented at American helicopter society 65th annual forum, Grapevine, Texas, 27–29 May 2009
15. Liggett ND, Smith MJ (2012) Temporal convergence criteria for time accurate viscous simulations of separated flows. Comput Fluids, Elsevier, 06:140–156